Impact of Oxygen Partial Pressure on the Ruddlesden−Popper Series $Nd_{2-2x}Sr_{1+2x}Mn_2O_7$: Oxygen Vacancy Formation and Ordering

Julie E. Millburn and John F. Mitchell*

Materials Science Division, Argonne National Laboratory, Argonne, Illinois 60439

Received December 28, 1999. Revised Manuscript Received April 17, 2001

The phase diagram of the $Nd_{2-2x}Sr_{1+2x}Mn_2O_{7+\delta}$ $n = 2$ Ruddlesden−Popper series has been investigated as a function of composition and oxygen partial pressure at 1400 °C. The regions of phase stability for $0.10 \leq x \leq 0.70$ and $10^{-6} \leq p(O_2)/\text{atm} \leq 1.0$ have been mapped out and a systematic relationship between x and oxygen partial pressure established. At high $p(O_2)$ (near 1 atm) the upper solubility limit is fixed by an average Mn oxidation state of +3.5, while the lower limit of stability is a strong function of $p(O_2)$. Phases synthesized at low $p(O_2)$ are associated with the introduction of oxygen vacancies that can be filled at low temperature to yield metastable phases with formal Mn oxidation states beyond +3.5. The oxygen vacancy structures are highly dependent on the Nd/Sr ratio, with the location of the vacancies changing from in-plane to axial as a function of both x and temperature. Systematic study of the Mn−O bonding framework reveals a subtle dependence of the crystal structure on both the Mn oxidation state and vacancy location. The unusual crystal chemistry of these phases suggests a more general synthetic technique for accessing layered manganite phases as potential CMR candidates.

Introduction

Mixed-valent manganite perovskites have received considerable attention among solid state scientists, primarily because of their colossal magnetoresistance (CMR) but more generally due to the unusually strong coupling between their lattice, spin, and charge degrees of freedom.[1−3] Although the majority of research has focused on the pseudocubic $Ln_{1-x}A_xMnO_3$ perovskites (A = Ca, Sr, Ba, Pb, Bi), naturally layered CMR materials from the $n = 2$ Ruddlesden−Popper series have also attracted attention because of their potential as model systems for low-dimensional physics.[4−6] They are also attractive from any putative technological standpoint because they exhibit substantially better low-field magnetoresistance than their three-dimensional perovskite counterparts.[7]

The majority of research in the tetragonal $I4/mmm$ $n = 2$ layered systems has centered on the $La_{2-2x}Sr_{1+2x}Mn_2O_{7+\delta}$ series, where metal−insulator transitions have been found in the range $0.3 \leq x \leq 0.5$.[7−11] Substitution of Nd for La in this composition range destroys the occurrence of the metal−insulator transition.[12] In an attempt to recover this electronic transition at compositions outside the $0.3 \leq x \leq 0.5$ region, we have systematically studied the effect of synthesis atmosphere on the phase formation and crystal chemistry of the $Nd_{2-2x}Sr_{1+2x}Mn_2O_{7+\delta}$ system. In particular, we report here the effect of variation in oxygen partial pressure during synthesis upon the phase diagram of $Nd_{2-2x}Sr_{1+2x}Mn_2O_{7+\delta}$ in the region $0.1 \leq x \leq 0.7$ and how atmospheric control can be used to access compositions both above $x = 0.5$ and below $x = 0.3$. As a result of this investigation, we report an unexpected oxygen vacancy structure formed at low $p(O_2)$. In this defect structure oxygen vacancies preferentially locate in the MnO_2 plane or in apical positions depending upon temperature and composition. The appearance of preferential in-plane ordering of these vacancies in the $x = 0.6$ compound represents a novel crystal chemistry in $n = 2$ manganite Ruddlesden−Popper phases and illustrates the sensitivity of the anion sublattice to the underlying metal framework.

Experimental Section

Polycrystalline 5-g samples of $Nd_{2-2x}Sr_{1+2x}Mn_2O_{7+\delta}$, $0.1 \leq x \leq 0.7$, were prepared by high-temperature, solid-state reaction

* To whom correspondence should be addressed.

(1) Raveau, B.; Maignan, A.; Caignaert, V. *J. Solid State Chem.* **1995**, *117*, 424.
(2) Urushibara, A.; Moritomo, Y.; Arima, T.; Asamitsu, A.; Kido, G.; Tokura, Y. *Phys. Rev. B* **1995**, *51*, 14103.
(3) Radaelli, P. G.; Marezio, M.; Hwang, H. Y.; Cheong, S. W.; Batlogg, B. *Phys. Rev. B* **1996**, *54*, 8992.
(4) Moritomo, Y.; Tomioka, Y.; Asamitsu, A.; Tokura, Y.; Matsui, Y. *Phys. Rev. B* **1995**, *51*, 3297.
(5) Mitchell, J. F.; Argyriou, D. N.; Jorgensen, J. D.; Hinks, D. G.; Potter, C. D.; Bader, S. D. *Phys. Rev. B* **1996**, *55*, 63.
(6) Battle, P. D.; Hepburn, J. A.; Millburn, J. E.; Radaelli, P. G.; Rosseinsky, M. J.; Spring, L. E.; Vente, J. F. *Chem. Mater.* **1997**, *9*, 3215.
(7) Moritomo, Y.; Asamitsu, A.; Kuwahara, H.; Tokura, Y. *Nature* **1996**, *380*, 141.
(8) Kimura, T.; Tomioka, Y.; Asamitsu, A.; Tokura, Y. *Phys. Rev. Lett.* **1998**, *81*, 5920.
(9) Argyriou, D. N.; Mitchell, J. F.; Goodenough, J. B.; Chmaissem, O.; Short, S.; Jorgensen, J. D. *Phys. Rev. Lett.* **1997**, *78*, 1568.
(10) Perring, T. G.; Aeppli, G.; Moritomo, Y.; Tokura, Y. *Phys. Rev. Lett.* **1997**, *78*, 3197.
(11) Hirota, K.; Moritomo, Y.; Fujioka, H.; Kubota, M.; Yoshizawa, H.; Endoh, Y. *J. Phys. Soc. Jpn.* **1998**, *67*, 3380.
(12) Moritomo, Y.; Maruyama, Y.; Akimoto, T.; Nakamura, A. *Phys. Rev. B* **1997**, *56*, R7057.

10.1021/cm990809e CCC: $20.00
Published on Web 05/30/2001

Table 1. Gas Mixtures Employed during Synthesis at 1400 °C of $Nd_{2-2x}Sr_{1+2x}Mn_2O_{7+\delta}$ Samples $0.1 \le x \le 0.7$ and the Corresponding Oxygen Partial Pressures

gas mixture	$p(O_2)$ (atm)
99.99% O_2 in Ar	1.00
20.30% O_2 in Ar	0.203
1.02% O_2 in Ar	0.0102
0.105% O_2 in Ar	0.00105
400 ppm O_2 in Ar	0.0004
0.507% CO/19.63% CO_2 in N_2	3.9×10^{-6} [a]

[a] For the buffer gas mixture the corresponding $p(O_2)$ at 1400 °C is calculated using the method in ref 13.

of Nd_2O_3 (Johnson-Matthey REacton 99.99%, prefired at 1000 °C in air for 12 h), $SrCO_3$ (Johnson-Matthey Puratronic 99.994%, dried at 150 °C in air for 12 h), and MnO_2 (Johnson-Matthey Puratronic 99.999%, prefired at 425 °C in flowing oxygen for 6 h, and then slow cooled at 1 °C min^{-1} to room temperature). Stoichiometric quantities of the starting materials were mixed and fired in air at 900 °C for 12 h and then 1075 °C for an additional 30 h. The resulting powders were pressed into three 13-mm-diameter pellets at 6000 lb and annealed at 1300 °C for 48 h and then 1400 °C for 200 h, under flowing 20.3% O_2 in Ar. Approximately 500-mg portions of the black crystalline products obtained were subsequently pelletized and annealed at 1400 °C for 200 h under a variety of gas mixtures (AGA) corresponding to oxygen partial pressures in the range $10^{-6} \le p(O_2)$ (atm) ≤ 1.0; precise values are given in Table 1. For oxygen-based atmospheres the nominal $p(O_2)$ expected was confirmed by means of an oxygen sensor inserted into the furnace during synthesis. For each gaseous atmosphere the furnace apparatus was thoroughly purged for a minimum of 4 h at room temperature before heating was commenced. In all cases, pelletized samples were ramped to and from the given temperature under the corresponding gas flow at a rate of 4 °C min^{-1} and materials were reground between each firing. Long firing times were employed to ensure that reactions had proceeded to equilibrium. Qualitative progress of the reactions was monitored by room-temperature powder X-ray diffraction of the products at various stages during synthesis, using a Rigaku rotating anode diffractometer operating in reflection geometry.

In addition, 20-g samples of the $x = 0.6$ and 0.7 compositions, $Nd_{0.8}Sr_{2.2}Mn_2O_{7+\delta}$ and $Nd_{0.6}Sr_{2.4}Mn_2O_{7+\delta}$, were prepared for powder neutron diffraction studies, using the lowest $p(O_2)$ of $\approx 4 \times 10^{-6}$ atm, corresponding to the 0.507% CO/19.63% CO_2 in N_2 buffer gas.[13] Portions of each of these two larger samples were subsequently annealed at 500 °C in pure oxygen for 5 h. The Mn^{4+} content of the as-made and annealed materials was determined by iodometric titration against a standardized sodium thiosulfate solution. For each composition titrations were repeated several times to ensure accurate and consistent results (typically less than a 2% spread). Approximately 50-mg portions of as-made materials were also rapidly heated on a thermogravimetric analysis (TGA) balance to 450 °C in flowing oxygen, held at this temperature until no further weight change was observed, then quickly cooled to room temperature.

Room-temperature time-of-flight (TOF) powder neutron diffraction data were collected for the as-made and O_2 annealed 0.6 and 0.7 samples, contained in cylindrical vanadium cans, at Argonne National Laboratory's Intense Pulsed Neutron Source (IPNS), on the Special Environment Powder Diffractometer (SEPD) ($\pm 145°$ 2θ, $0.41 \le d/Å \le 3.96$, $\Delta d/d$ (fwhm) = 0.0034). For the $x = 0.6$ composition data were also collected as a function of temperature on SEPD using a Miller furnace ($\pm 90°$ 2θ, $0.57 \le d/Å \le 5.41$, $\Delta d/d$ (fwhm) = 0.0054). For these measurements two 13-mm-diameter, 8-mm-thick, 5-g pellets of the as-made $Nd_{0.8}Sr_{2.2}Mn_2O_{6.47}$ compound were suspended in the furnace within a quartz bucket, designed to allow gas flow around the sample pellets. Data were then collected at a range of temperatures between 25 and 600 °C as the sample was slowly heated under an ≈2 scft min^{-1} flow of the synthesis gas, 0.507% CO/19.63% CO_2 in N_2. After several hours at 600 °C, the gas flow was switched to 99.99% O_2 for a similar length of time, before being switched back to the original buffer mixture. The sample was then held at 600 °C for ≈18 h before being cooled slowly to room temperature still under the gas flow. All crystal structure analysis of the diffraction data was performed by the Rietveld method using the GSAS program suite.[14]

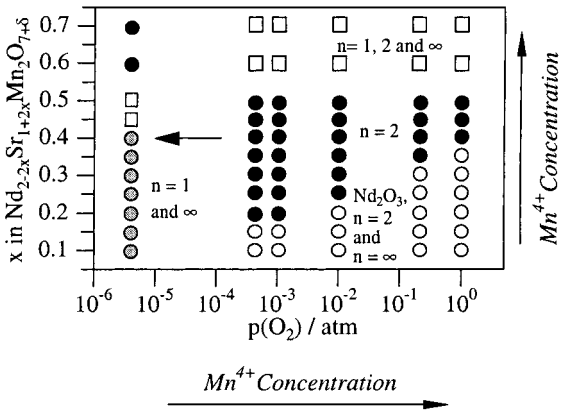

Figure 1. Schematic diagram showing the effect of $p(O_2)$ on the phase stability of $Nd_{2-2x}Sr_{1+2x}Mn_2O_7$ with $0.1 \le x \le 0.7$. Filled circles indicate successful single $n = 2$ phase synthesis.

Results and Discussion

Effects of $p(O_2)$. The phase diagram of the $Nd_{2-2x}Sr_{1+2x}Mn_2O_{7+\delta}$ series depends strongly on both composition, x, and oxygen partial pressure, $p(O_2)$. As shown in Figure 1, in ambient oxygen partial pressures ($p(O_2) = 0.203$ atm), single-phase $n = 2$ material could only be produced in the narrow composition range between $0.35 \le x \le 0.5$. For compositions with $x > 0.5$ (i.e., nominal Mn oxidation states greater than +3.5) $n = 1$ K_2NiF_4-type and $n = \infty$ perovskite phases are also observed as impurities along with the $n = 2$ material. For compositions with $x < 0.35$ (i.e., nominal Mn oxidation states lower than +3.35) $n = \infty$ and Nd_2O_3 impurity phases are obtained. Increasing the oxygen partial pressure to 1.0 atm (99.99% O_2 in Ar) narrows the $n = 2$ single-phase region even further such that pure $n = 2$ material is obtained only for $0.4 \le x \le 0.5$. However, by successively lowering the oxygen partial pressure during synthesis from 1.0 to 4×10^{-4} atm (400 ppm O_2 in Ar), it is possible to systematically extend the $n = 2$ single-phase composition range to lower values of x (i.e., to lower Mn oxidation states). At 4×10^{-4} atm, uncontaminated $n = 2$ material can be synthesized for compositions with $0.2 \le x \le 0.5$. It is worth noting that the upper compositional boundary of the single $n = 2$ phase region, $x = 0.5$, remains unchanged across this entire range of oxygen partial pressure. The effects of the changes in $p(O_2)$ on the powder X-ray diffraction pattern of products obtained for synthesis of the $x = 0.2$ composition are shown in Figure 2, and the variation in products obtained as a function of composition at a given $p(O_2)$, in this case 0.0102 atm, in Figure 3.

In an attempt to extend the solubility limit to $x < 0.2$ a 0.507% CO/19.63% CO_2 in N_2 buffer gas was employed

(13) DeHoff, R. T. In *Thermodynamics In Materials Science*; McGraw-Hill: New York, 1993; pp 322−366.

(14) Larson, A. C.; von Dreele, R. B. *General Structure Analysis System*; University of California: 1985−1990.

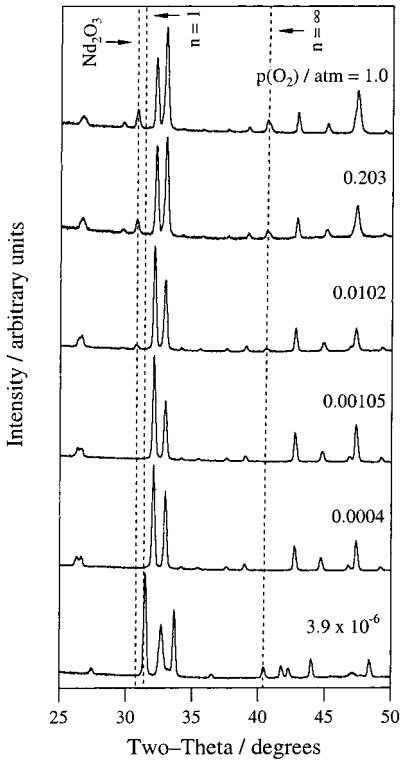

Figure 2. Powder X-ray diffraction patterns of the products obtained for the $x = 0.2$ composition, as a function of oxygen partial pressure during synthesis at 1400 °C for 200 h.

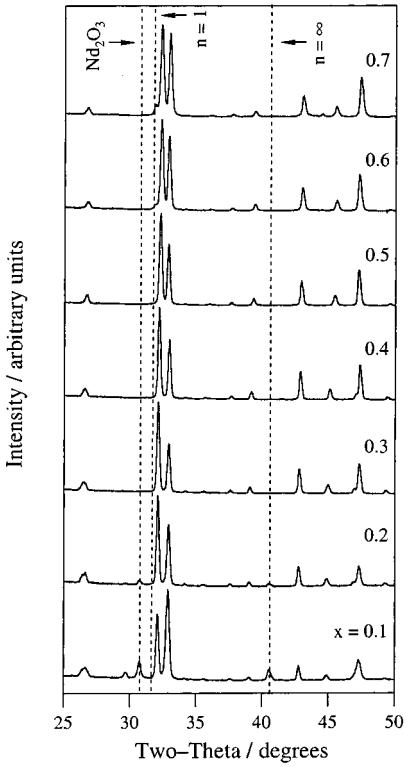

Figure 3. Powder X-ray diffraction patterns of the products obtained during synthesis of $Nd_{2-2x}Sr_{1+2x}Mn_2O_{7+\delta}$ samples at 1400 °C in a $p(O2) = 0.0102$ atm as a function of composition, x.

during synthesis. At 1400 °C the buffer gas produces an oxygen partial pressure of $\approx 4 \times 10^{-6}$ atm.[13] Contrary to the expected trend, however, in this much lower $p(O_2)$, uncontaminated $n = 2$ phase synthesis is achieved

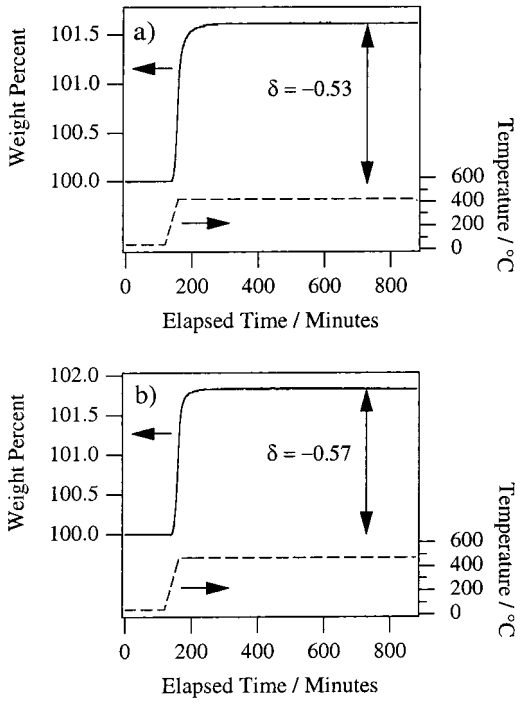

Figure 4. Thermogravimetric analysis in 100% O_2 of (a) $x = 0.6$ $Nd_{0.8}Sr_{2.2}Mn_2O_{7+\delta}$ and (b) $x = 0.7$ $Nd_{0.6}Sr_{2.4}Mn_2O_{7+\delta}$, prepared at 1400 °C in 0.507% CO/19.63% CO_2 in N_2.

for compositions with $0.6 \leq x \leq 0.7$, while those with $0.45 \leq x \leq 0.50$ contain $n = \infty$ and Nd_2O_3 impurities as well as the $n = 2$ phase material. Furthermore, for $x \leq 0.4$ a mixture of $n = 1$ and $n = \infty$ phases are obtained with no $n = 2$ material detectable by X-ray diffraction. Considering these observations, formation of the relatively high manganese oxidation states of +3.6 and +3.7, respectively, required to obtain stoichiometric, $\delta = 0$, $x = 0.6$ and 0.7 samples would seem unlikely under the considerably reducing conditions of the buffer gas. The successful synthesis of single $n = 2$ phases for these compositions in this atmosphere therefore suggests that the products obtained must in fact contain Mn in considerably lower oxidation states than those corresponding to the stoichiometric formulas. The most plausible means of achieving this would be the existence of a substantial number of oxygen vacancies in the as-made materials.

TGA results for the $x = 0.6$ and $x = 0.7$ samples produced in the buffer gas corroborate this hypothesis. As can be seen in Figure 4, within 3 h at 450 °C under flowing oxygen the weight gain of both samples saturates. Assuming the endpoint mass corresponds to the stoichiometric $\delta = 0$ materials, that is, $Nd_{0.8}Sr_{2.2}Mn_2O_{7.0}$ and $Nd_{0.6}Sr_{2.4}Mn_2O_{7.0}$, then the as-made materials may be formulated as $Nd_{0.8}Sr_{2.2}Mn_2O_{6.47}$ and $Nd_{0.6}Sr_{2.4}Mn_2O_{6.43}$ respectively, corresponding to $\delta = -0.53$ ($Mn^{3.07+}$) and -0.57 ($Mn^{3.13+}$). Independent confirmation of these oxygen contents was provided by iodometric titration, which gave values of $\delta = -0.53 \pm 0.01$ for the $x = 0.6$ sample and $\delta = -0.58 \pm 0.01$ for the $x = 0.7$ sample, in excellent agreement with the TGA results. In addition, iodometric titrations performed on portions of these as-made $x = 0.6$ and 0.7 samples, which had been subsequently annealed at 500 °C in pure oxygen for 5 h, showed both materials to be stoichiometric, $\delta = 0.00 \pm 0.01$.

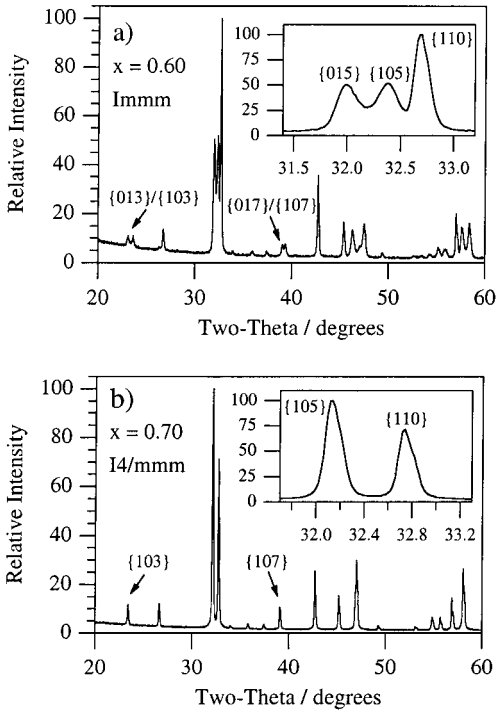

Figure 5. Powder X-ray diffraction data for (a) $Nd_{0.8}Sr_{2.2}Mn_2O_{6.47}$ and (b) $Nd_{0.6}Sr_{2.4}Mn_2O_{6.42}$ prepared at 1400 °C in 0.507% CO/19.63% CO_2 in N_2, showing the peaks that split upon lowering of the symmetry from *I*4/*mmm* ($x = 0.7$) to *Immm* ($x = 0.6$).

***x* = 0.6 and 0.7: Powder Neutron Diffraction Data.** While the $x = 0.7$ sample is tetragonal, the X-ray diffraction pattern of the $x = 0.6$, $Nd_{0.8}Sr_{2.2}Mn_2O_{7+\delta}$, sample prepared in the buffer gas shows splitting of some Bragg reflections, indicative of an orthorhombic unit cell (see Figure 5). Two distortions of the *I*4/*mmm* cell to orthorhombic symmetry are known, depending on which of the ⟨100⟩ and ⟨110⟩ sets of mirror planes and 2-fold axes are lost along with the 4-fold axis when the symmetry is lowered. The most commonly observed distortion involves a doubling of the cell size in a $(\sqrt{2}a) \times (\sqrt{2}b) \times c$ superstructure, with a 45° rotation about *c*, in which the face diagonals of the *I*4/*mmm* cell become the new cell vectors and the ⟨100⟩ mirror planes are lost. The signature of this in powder diffraction is a splitting of the tetragonal {*hhl*} (into {2*h*, 0, *l*} and {0, 2*h*, *l*}) and {*hkl*} reflections (into {$h + k$, $h - k$, *l*} and {$h - k$, $h + k$, *l*}) while the {*h*0*l*} reflections remain unsplit (as {*hhl*} in the enlarged cell). This is found in the $n = 1$ Ruddlesden−Popper high-temperature superconducting cuprates, in $La_2NiO_{4\pm\delta}$[15] and many other K_2NiF_4 structure oxides, resulting in structures with the space group symmetries *Cmca* (tilting of MO_6 octahedra through a small angle about the *b* axis) or *Fmmm* (positive distortion of the MO_6 octahedra along the *b* direction). Inspection of the X-ray diffraction pattern of $Nd_{0.8}Sr_{2.2}Mn_2O_{7+\delta}$ indicates that this is not the case: Figure 5a shows that the *I*4/*mmm* {105} reflection splits while the {110} does not. An alternative distortion results in the loss of the ⟨110⟩ mirror planes and produces an orthorhombic cell of the same volume in which the *a* and *b* cell directions are retained, but are no longer equivalent

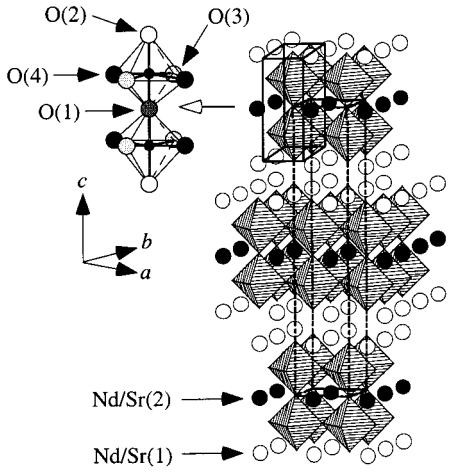

Figure 6. Diagram of the $n = 2$ Ruddlesden−Popper $Nd_{2-2x}Sr_{1+2x}Mn_2O_7$ structure showing the bilayers of MnO_6 octahedra and two distinct A cation sites in the unit cell. Also shown is an enlargement of the bilayer, illustrating the four different oxygen positions available in the orthorhombic *Immm* structure, $a_O \neq b_O$. (In *I*4/*mmm* $a_T = b_T$ and O(3) and O(4) are equivalent.)

in magnitude. Such a distortion has been reported for mixed valence, reduced $n = 1$ K_2NiF_4-type nickelates, $La_{1.6}Sr_{0.4}(Ni^{I}, Ni^{II})O_{3.47}$,[16] $LaSr(Ni^{I}, Ni^{II})O_{3.1}$,[17] $LaSrCr_xNi_{1-x}O_{4+\delta}$ ($x = 0.1$, 0.2),[18] and other $La_{2-x}Sr_xNiO_{4-\delta}$ samples with $\delta > 0$ and $0.1 < x \leq 0.5$,[19] where the oxygen vacancies are found solely in the NiO_x planes. These compounds have orthorhombic symmetry due to the oxygen vacancies occurring preferentially along one axis within the MO_x layers. In this case the {*hhl*} reflections remain degenerate whereas the {*h*0*l*} split into {0*hl*} and {*h*0*l*}. The observation of such a pattern of splittings for the $x = 0.6$ material suggests it adopts this structure, describable in the *Immm* space group.

Synthesis of additional samples with $0.5 < x < 0.7$ suggests that single $n = 2$ phase synthesis under a $p(O_2)$ of $\sim 4 \times 10^{-6}$ atm is achieved for compositions in the approximate region $0.55 < x < 0.72$, with an orthorhombic distortion of the $n = 2$ structure occurring only in the narrow composition range $0.55 < x < 0.62$. 20 g samples of both the $x = 0.6$ and $x = 0.7$ compositions were prepared to investigate the location of the oxygen vacancies and the nature of the orthorhombic distortion within the as-made materials by powder neutron diffraction.

The very similar neutron scattering lengths of Nd and Sr (7.69 and 7.02 fm, respectively) result in the refinements being highly insensitive to any variation in the relative distribution of the cations over the two available A cation sites in the unit cell (see Figure 6). Consequently, because it was impossible to reliably refine any potential ordering, the A cation ratios in the final refinements were simply fixed at those values corresponding to a statistical distribution in line with the

(15) Rodriguez-Carvajal, J.; Fernandez-Diaz, M. T.; Martinez, J. L. *J. Phys.: Condens. Matter* **1991**, *3*, 3215.

(16) Crespin, M.; Bassat, J. M.; Odier, P.; Mouron, P.; Choisnet, J. *J. Solid State Chem.* **1990**, *84*, 165.

(17) Crespin, M.; Landron, C.; Odier, P.; Bassat, J. M.; Mouron, P.; Choisnet, J. *J. Solid State Chem.* **1992**, *100*, 281.

(18) Millburn, J. E.; Rosseinsky, M. J. *Chem. Mater.* **1997**, *9*, 511.

(19) Medarde, M.; Rodriguez-Carvajal, J.; Obradors, X.; Vallet-Regi, M.; Gonzalez-Calbet, J. M.; Sayagues, M. J. *Physica B* **1992**, *180*−*181*, 399.

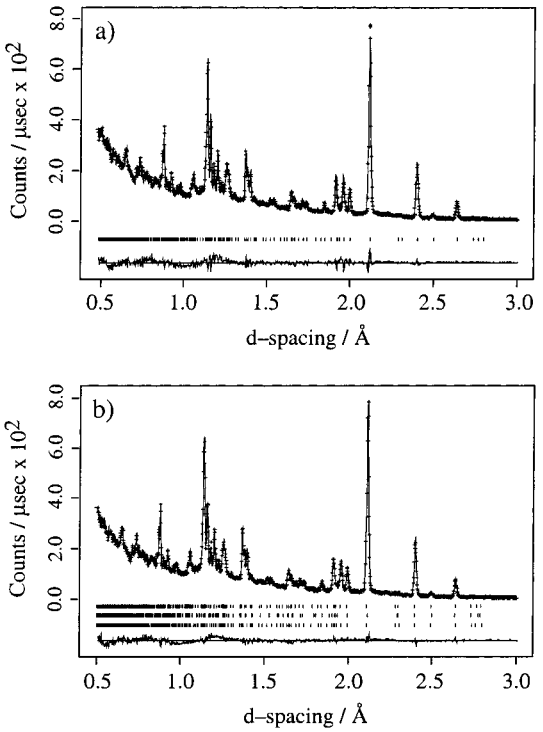

Figure 7. Observed (markers), calculated, and difference profiles for Rietveld refinement of room-temperature powder neutron diffraction data for $Nd_{0.8}Sr_{2.2}Mn_2O_{6.47}$ using (a) a single *Immm* phase model and (b) a three *Immm* phase model.

chemical composition of the sample in question, that is, Nd:Sr = 27:73% for $x = 0.6$ and 20:80% for $x = 0.7$.

Rietveld refinement of the room-temperature powder neutron diffraction data for the $x = 0.6$ and $\delta = -0.53$ sample reveals a phase mixture. As can be seen in Figure 7 a), a single-phase Rietveld refinement of the data in *Immm* results in an unsatisfactory fit. Detailed inspection of the fit to the peaks that are split upon lowering of the symmetry from tetragonal to orthorhombic indicates the presence of diffracted intensity between them: the intensity does not fall to the background level, suggesting the presence of more than one phase within the sample (see Figure 8 a). This multiphasic behavior should be distinguished from that previously reported for $x = 0.4$ and $x = 0.5$ compositions.[20,6] In these latter materials, coexistence of two Ruddlesden−Popper phases with very similar unit cell volumes, which differ only in the distribution of Sr^{2+} and Nd^{3+} cations over the two A cation sites, gives rise to a subtle phase separation, which is established from broadening of the {0010} reflection because this reflection cannot be split by lowering the space group symmetry.

Multiphase refinement of the data for the as-made $x = 0.6$ sample was attempted employing a variety of models incorporating combinations of several orthorhombic *Immm* and tetragonal *I*4/*mmm* phases. Attempts to include more than three phases into the model always proved unstable, while refinement with any combination of only two phases did not result in satisfactory agreement. Therefore, the final refinements

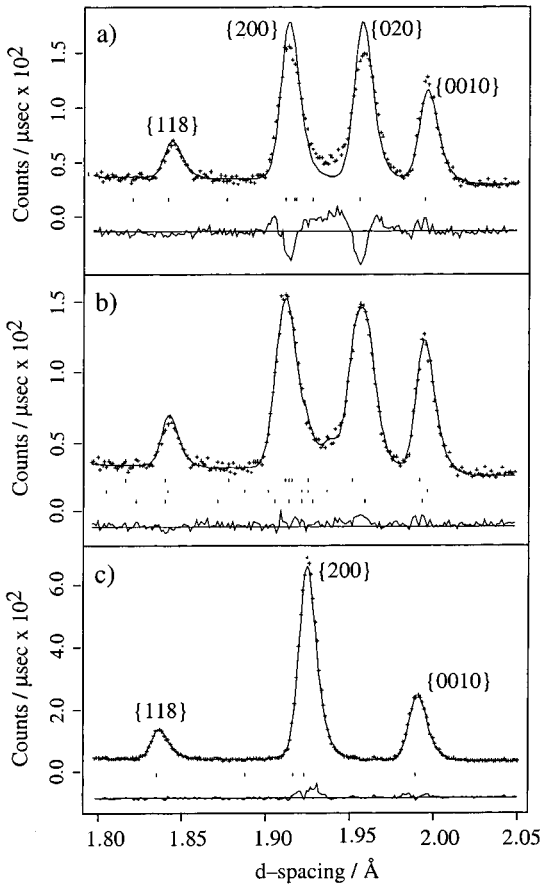

Figure 8. Enlargement over the *d*-spacing region 1.80−2.05 Å of the observed, calculated, and difference profiles for Rietveld refinement of room-temperature powder neutron diffraction data for $Nd_{0.8}Sr_{2.2}Mn_2O_{7+\delta}$ for (a) an as-made $\delta = -0.53$, single *Immm* phase model, (b) an as-made $\delta = -0.53$, three *Immm* phase model, and (c) a low-temperature oxygen annealed $\delta = 0$, single *I*4/*mmm* phase model.

were performed using a three *Immm* phase model, ultimately resulting in a reduction of χ^2 from 3.53 (single *Immm* phase) to 2.24 (three *Immm* phases) (see Figures 7b and 8b). The lattice parameters, phase fractions, and oxygen site occupancies for each phase were successfully refined independently of one another. Because of significant correlations among the large number of variable parameters involved, it proved necessary to constrain the peak widths, isotropic temperature factors, and atomic coordinates of the atoms to be the same within each of the three phases. In addition, the site occupancy of the O(3) in-plane oxygen atom, which lies along the crystallographic *b* axis of the unit cell (see Figure 6), consistently refined to unity for all three phases and so was fixed at 1.0 in the final refinement, results of which are given in Table 2.

Although the number of constraints employed and correlations between the oxygen site occupancies and temperature factors make quantitative analysis of the results problematic, refinement of the oxygen content of the three phases does lead to values, which when combined with the appropriate mole fractions of each phase, give a calculated overall stoichiometry corresponding to $Nd_{0.8}Sr_{2.2}Mn_2O_{6.56}$, or $\delta = -0.44$, in reasonable agreement with that obtained from TGA and iodometry of $Nd_{0.8}Sr_{2.2}Mn_2O_{6.47}$, or $\delta = -0.53$. Furthermore, it appears that, for the two majority phases, phase

(20) Battle, P. D.; Green, M. A.; Laskey, N. S.; Millburn, J. E.; Murphy, L. E.; Rosseinsky, M. J.; Sullivan, S. P.; Vente, J. F. *Chem. Mater.* **1997**, *9*, 552.

Table 2. Structural Parameters Obtained from Three-Phase Rietveld Refinement of Room-Temperature Powder Neutron Diffraction Data for $x = 0.6$, $\delta = -0.53(1)$ $Nd_{0.8}Sr_{2.2}Mn_2O_{6.47}$ Prepared at 1400 °C in 0.507% CO/ 19.63% CO_2 in N_2[a]

	phase[b]	1	2	3
phase fraction		39.2%	11.8%	49.0%
a (Å)		3.8150(7)	3.847(1)	3.8266(7)
b (Å)		3.9209(9)	3.877(1)	3.9055(9)
c (Å)		19.940(7)	19.990(9)	19.935(5)
Nd/Sr(1)	U_{iso} (Å^2)	0.017(9)	0.017(9)	0.017(9)
Nd/Sr(2)	*z*	0.3182(1)	0.3182(1)	0.3182(1)
	U_{iso} (Å^2)	0.017(9)	0.017(9)	0.017(9)
Mn	*z*	0.0972(2)	0.0972(2)	0.0972(2)
	U_{iso} (Å^2)	0.0017(8)	0.0017(8)	0.0017(8)
O(1)	U_{iso} (Å^2)	0.047(5)	0.047(5)	0.047(5)
	occupancy	0.82(8)	0.6(1)	0.67(6)
O(2)	*z*	0.1955(2)	0.1955(2)	0.1955(2)
	U_{iso} (Å^2)	0.012(1)	0.012(1)	0.012(1)
	occupancy	1.02(3)	0.63(8)	0.97(3)
O(3)	*z*	0.0913(1)	0.0913(1)	0.0913(1)
	U_{iso} (Å^2)	0.020(1)	0.020(1)	0.020(1)
	occupancy	1.0[c]	1.0[c]	1.0[c]
O(4)	*z*	0.0913(1)	0.0913(1)	0.0913(1)
	U_{iso} (Å^2)	0.021(2)	0.021(2)	0.021(2)
	occupancy	0.97(5)	0.93(8)	0.95(4)
R_{wp} (%)			7.15	
R_p (%)			5.04	

[a] Atoms were refined in the following Wyckoff positions of space group no. 71, *Immm*: 2Sr(1)/Nd(1), in (c), (*mmm*) (0, 0, $^1/_2$); 4Sr(2)/ Nd(2), 4Mn, and 4O(2), in (i), (*mm*2) (0, 0, *z*); 2O(1), in (a), (*mmm*) (0, 0, 0); 4O(3), in (j), (*mm*2) (0, $^1/_2$, *z*); 4O(4), in (j), (*mm*2) ($^1/_2$, 0, *z*). [b] Some parameters were constrained as described in the text. [c] Occupancy fixed at 1.0 as described in the text.

1 (39.2%) and phase 3 (49.0%), which have very similar *c* lattice parameters, the oxygen vacancies occur exclusively at the O(1) position, corresponding to the apical oxygen atom shared between the MnO bilayers, and the O(4) position, corresponding to the in-plane oxygen atom lying along the *a* axis. However, for the minority phase, phase 2 (11.8%), which has a much larger *c* lattice parameter, there also appear to be a significant number of vacancies at the O(2) position, corresponding to the apical oxygen atom that sticks out into the Nd/Sr−O rock salt layers (see Table 2 and Figure 6).

Data collected following the low-temperature, oxygen annealing of the as-made material support assignment of the cause of the *Immm* orthorhombic distortion in the $\delta = -0.53$ sample to preferential occurrence of oxygen vacancies along the *a* axis within the MnO_2 layers. As can be seen in Figures 8c and 9a, the structure reverts to being tetragonal upon oxygenation; that is, when there are no longer any vacancies, $\delta = 0$, there no longer exists a lowering of symmetry. Importantly, room-temperature powder neutron diffraction data for this $\delta = 0$ stoichiometric tetragonal compound can be satisfactorily refined using a single *I*4/*mmm* phase model; results of the refinement are given in Table 3. These results lead us to conclude that the multiphasic nature of the as-made sample is due to inhomogeneity in the distribution and concentration of the oxygen vacancies across the material.

Upon oxidation of the orthorhombic phase, both the *c* and *a* lattice parameters contract, relative to the *c* and average in-plane orthorhombic lattice parameter, respectively. This reduction in unit cell size is consistent with the expected decrease in MnO_6 octahedral volume associated with the increase in the Mn oxidation state from +3.07 ($\delta = -0.53$) to +3.60 ($\delta = 0.00$) upon filling

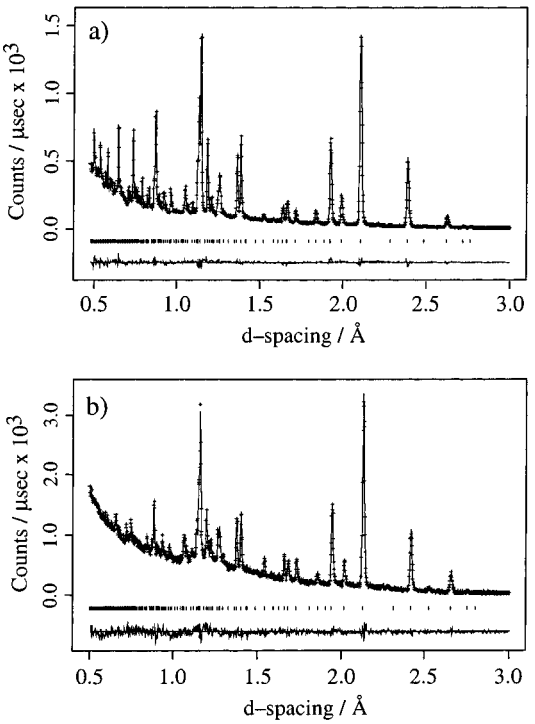

Figure 9. Observed (markers), calculated, and difference profiles for Rietveld refinement of powder neutron diffraction data using a single *I*4/*mmm* phase model for $Nd_{0.8}Sr_{2.2}Mn_2O_{7+\delta}$: (a) low-temperature oxygen annealed $\delta = 0$ room-temperature data and (b) as-made $\delta = -0.53$ 600 °C data.

of the vacancies. Refinement of the oxygen site occupancies for the O_2 annealed sample leads to full occupancy of the in-plane O(3) and apical O(1) positions, within error, in accordance with the TGA and iodometry results, but to reduced occupancy at the O(2) position, corresponding to the apical oxygen that projects into the rock-salt layer (see Figure 6). Although the results of refinement are initially somewhat surprising in view of the stoichiometry established by chemical means, closer inspection reveals that refinement also produces a temperature factor at this site somewhat smaller than those for the other oxygen atoms, suggesting a possible correlation between the two parameters at the O(2) position. Indeed, fixing the occupancy at 1.0 has no significant effect upon either the overall goodness of fit or the values of parameters describing the other atoms within the unit cell.

For the $x = 0.7$ composition, the room-temperature powder neutron diffraction data for both the as-made, oxygen-deficient and oxygenated, stoichiometric compounds can be refined satisfactorily using a single-phase tetragonal *I*4/*mmm* phase model. Results of the refinements are given in Table 3 and the observed, calculated, and difference profiles in Figure 10a,b, respectively. As with the $x = 0.6$ sample, both the *a* and *c* lattice parameters contract upon filling of the vacancies, consistent with the accompanying increase in Mn oxidation state from +3.13 ($\delta = -0.57$) to +3.70 ($\delta = 0.0$). However, the total oxygen content obtained from refinement of the data for the as-made $x = 0.7$ material is significantly greater than that obtained from the TGA and iodometry measurements; that is, the number of vacancies is significantly less, $\delta \approx -0.4$ rather than −0.57. As shown in Table 3, the refined oxygen vacancies occur exclusively in the apical O(1) position, corre-

Table 3. Structural Parameters Obtained from Rietveld Refinement of Powder Neutron Diffraction Data Collected at Room Temperature and 600 °C, for $x = 0.6$ and $x = 0.7$ $Nd_{2-2x}Sr_{1+2x}Mn_2O_{7+\delta}$ Samples, Both As-Made at 1400 °C in 0.507% CO/19.63% CO_2 in N_2 ($\delta < 0$), and Then Oxygen Annealed at 500 °C ($\delta = 0$)[a]

	x	0.7	0.7	0.6	0.6	0.6
	δ	−0.58(1)	0.00(1)	0.00(1)	−0.53(1)	0.00(1)
	temperature	RT	RT	RT	600 °C	600 °C
	a (Å)	3.86179(6)	3.83833(3)	3.84479(5)	3.8901(1)	3.86734(5)
	c (Å)	20.039(1)	19.9095(2)	19.8815(4)	20.188(1)	20.0685(5)
Nd/Sr(1)	U_{iso} (Å^2)	0.018(1)	0.0047(2)	0.0051(6)	0.023(2)	0.0134(9)
Nd/Sr(2)	z	0.3165(1)	0.31678(8)	0.31757(9)	0.3168(2)	0.3172(1)
	U_{iso} (Å^2)	0.0108(9)	0.0063(3)	0.0090(5)	0.020(2)	0.0196(9)
Mn	z	0.970(2)	0.0970(1)	0.0971(1)	0.0979(4)	0.0974(2)
	U_{iso} (Å^2)	0.011(1)	0.0025(3)	0.0014(4)	0.011(1)	0.0064(6)
O(1)	U_{iso} (Å^2)	0.055(4)	0.0141(9)	0.015(1)	0.068(7)	0.035(2)
	occupancy	0.75(2)	1.06(1)	1.00(1)	0.75(3)	1.03(1)
O(2)	z	0.1945(2)	0.1937(1)	0.1944(1)	0.1947(4)	0.1941(2)
	U_{iso} (Å^2)	0.022(2)	0.0080(5)	0.0080(7)	0.026(3)	0.014(1)
	occupancy	0.98(1)	0.970(5)	0.931(9)	0.87(1)	0.89(1)
O(3)	z	0.0913(1)	0.09521(7)	0.09572(9)	0.0918(2)	0.0955(1)
	U_{iso} (Å^2)	0.030(1)	0.0109(3)	0.0108(4)	0.036(2)	0.0232(8)
	occupancy	0.97(1)	1.036(8)	1.002(7)	1.01(3)	1.016(9)
	R_{wp} (%)	7.10	7.38	5.97	6.88	5.66
	R_p (%)	5.00	5.04	3.89	4.99	3.73

[a] Atoms were refined in the following Wyckoff positions of space group no. 139, *I*4/*mmm*: 2Sr(1)/Nd(1), in (b), (4/*mmm*) (0, 0, $^1/_2$); 4Sr(2)/Nd(2), 4Mn, and 4O(2), in (e), (4*mm*) (0, 0, *z*); 2O(1), in (a), (4/*mmm*) (0, 0, 0); 8O(3), in (g), (2*mm*) (0, $^1/_2$, *z*).

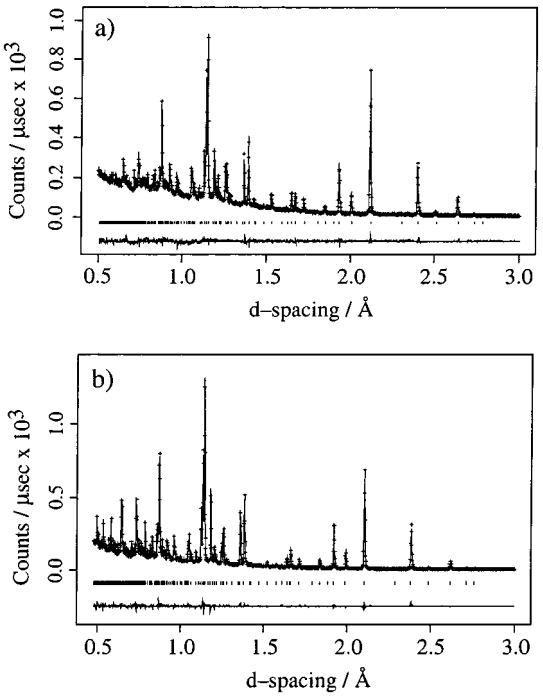

Figure 10. Observed (markers), calculated, and difference profiles for Rietveld refinement of room-temperature powder neutron diffraction data, using a single *I*4/*mmm* phase model, for $Nd_{0.6}Sr_{2.4}Mn_2O_{7+\delta}$: (a) as-made $\delta = -0.53$ and (b) low-temperature oxygen annealed $\delta = 0$.

sponding to the oxygen atom shared between the bilayers (see Figure 6). This arrangement is commonly found for other oxygen-deficient $n = 2$ and $n = 3$ Ruddlesden−Popper phases such as $Sr_3V_2O_{7-\delta}$,[21] $Sr_4V_3O_{10-\delta}$,[22] $Sr_3Fe_2O_{7-\delta}$,[23] $Sr_3Co_2O_{6.06}$,[24] and $La_{1.6}Sr_{0.4}CaCu_2O_6$.[25] While there appear to be no additional vacancies at either the in-plane O(3) or apical O(2) position, within error, the occupancy of the latter site actually refines to less than unity (occupancy = 0.970(5)) for the annealed $\delta = 0$ sample, as was the case for the stoichiometric $x = 0.6$ sample at both 600 °C and room temperature. Likewise, refinement also produces a comparatively small temperature factor at the O(2) position compared to those of the other oxygen atoms, suggesting a persistent correlation problem between the temperature factor and occupancy for this site in all cases. Because the Mn−O(2) bond is directed away from the bilayer into the Nd/Sr−O rock-salt layer (see Figure 6), the difficulties encountered with refinement of parameters for the O(2) site may be the result of a nonstatistical A cation distribution not accounted for in the Rietveld model.

While the above correlation makes it difficult to establish unequivocally that there are no vacancies at the O(2) position in the as-made $x = 0.7$ material, comparison with the other refinement results make this conclusion probable. Assuming this to be the case, to eliminate the discrepancy between the refined number of vacancies and the value established by chemical methods, it is clearly necessary to introduce either additional vacancies at the O(1) site and/or vacancies within the plane at O(3). Unfortunately, the refinement is insufficiently sensitive to the requisite alterations in occupancy at these sites to differentiate between the various possibilities. Therefore, although there are undoubtedly a large number of oxygen vacancies situated between the MnO_2 planes, it is not possible to rule out the existence of some vacancies within the plane as well. The enduring tetragonal nature of the oxygen-deficient $x = 0.7$ sample indicates, however, that if the latter do exist, they are distributed randomly over the O(3) position, as is found for the $x = 1.0$ material $Sr_3Mn_2O_{6.45}$,[26] rather than preferentially ordered along one

(21) Itoh, M.; Shikano, M.; Kawaji, H.; Nakamura, T. *Solid State Commun.* **1991**, *80*, 545.
(22) Gong, W.; Xue, J. S.; Greedan, J. E. *J. Solid State Chem.* **1991**, *91*, 180.
(23) Dann, S. E.; Weller, M. T.; Currie, D. B. *J. Solid State Chem.* **1992**, *97*, 179.
(24) Dann, S. E.; Weller, M. T. *J. Solid State Chem.* **1995**, *115*, 499.
(25) Cava, R. J.; Santoro, A.; Krajewski, J. J.; Fleming, R. M.; Waszczak, J. V.; Peck, W. F., Jr.; Marsh, P. *Physica C* **1990**, *172*, 138.
(26) Mitchell, J. F.; Millburn, J. E.; Medarde, M.; Short, S.; Jorgensen, J. D. *J. Solid State Chem.* **1998**, *141*, 599.

axis, as for the $x = 0.6$ composition, which would lead to an analogous orthorhombic distortion.

In Situ Studies. To investigate the causes of the differences in oxygen-deficient structures for the $x = 0.7$ and $x = 0.6$ samples and to monitor the oxygen ordering process, powder neutron diffraction data for the $x = 0.6$ composition were collected as a function of temperature in the range $25 \leq T/°C \leq 600$.

When the as-made oxygen-deficient $x = 0.6$ material is heated to 600 °C in the 0.507% CO/19.63% CO_2 in N_2 buffer gas in which it was originally synthesized at 1400 °C, it undergoes an orthorhombic to tetragonal structural transition in the region $300 \leq T/°C \leq 460$. Isothermal data collected at 600 °C for the resultant tetragonal material can be satisfactorily refined using a single *I*4/*mmm* phase structural model. The results of the refinement are given in Table 3 and the observed, calculated, and difference profiles in Figure 9b. The results are very similar to those obtained at room temperature for the $x = 0.7/\delta = -0.53$ sample: full occupancy of the in-plane O(3) site, but a considerable number of defects at the apical O(1) position between the layers, and a refined total oxygen stoichiometry in excess of that measured by chemical methods, that is, fewer vacancies. As for the $x = 0.6/\delta = 0.0$ sample at room temperature, there also seems to be a number of vacancies on the other apical oxygen site, O(2), which because they remain when the sample is oxygenated, appear to be an artifact of the refinement, as previously discussed. Comparing the above results with those for the room temperature, multiphase refinement of the orthorhombic material, given in Table 2, suggests that upon heating the sample from room temperature to 600 °C the vacancies become mobile and are able to migrate from in-plane to apical positions within the structure. By 600 °C there are no remaining vacancies in the plane and thus no longer any orthorhombic distortion caused by preferential location of in-plane defects along the *a* axis. In addition, the increased mobility of the vacancies and lack of in-plane defects eliminates the multiphasic behavior found at room temperature, supporting the view that this is associated with inhomogeneities in the oxygen vacancy concentration and distribution within the compound.

Refinement of data collected at 600 °C after the gas is then switched to 99.99% O_2 in Ar shows that the now apical oxygen vacancies in the $x = 0.6$ sample rapidly fill at this temperature to yield the stoichiometric tetragonal material; no further changes are observed in the powder neutron diffraction pattern after ≈30 min, and oxidation is deemed complete at this point. Parameters obtained from refinement of data collected for the stoichiometric compound at 600 °C after this period of time are given in Table 3. The O(1) and O(3) site occupancies refine within error to unity in accordance with complete filling of the vacancies upon switching gases. In a comparison of the lattice parameters obtained for the stoichiometric and oxygen-deficient materials at 600 °C, both *a* and *c* contract upon oxidation, consistent with the accompanying increase in the Mn oxidation state.

The process of oxidation and reduction of the material at 600 °C is entirely reversible. When the gas is switched back to 0.507% CO/19.63% CO_2 in N_2 from

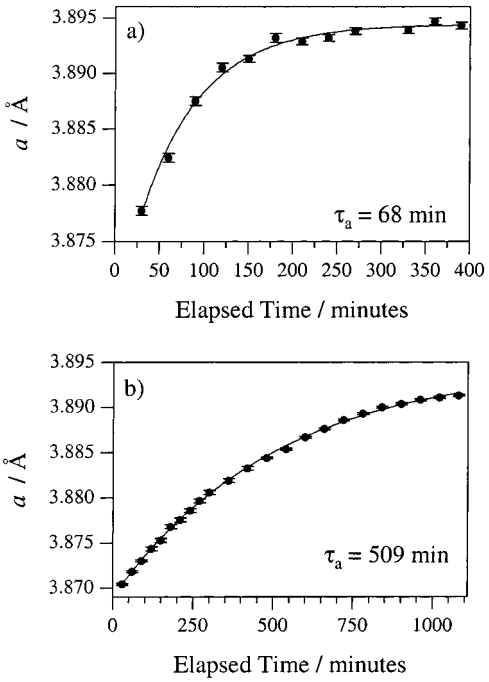

Figure 11. Evolution of the *a* lattice parameter upon formation of oxygen vacancies at 600 °C as a function of time for $Nd_{0.8}Sr_{2.2}Mn_2O_{7+\delta}$ samples: (a) single, 3-mm thick, 1-g pellet and (b) two, 9-mm-thick, 5-g pellets. Values of τ_a were obtained from fitting the data to $a(Å) = A + B \exp(-t/\tau_a)$. Analogous fits to the *c* lattice parameter data of both samples gave values of $\tau_c = 67$ and 591 min, respectively, consistent with those obtained for τ_a.

99.99% O_2 in Ar and the structure monitored at 600 °C, the tetragonal, oxygen-deficient material is recovered. It must be noted however that the length of time taken for the sample to equilibrate in the low $p(O_2)$ atmosphere, that is, that taken to form the vacancies, is considerably greater than that needed in the high $p(O_2)$ atmosphere to fill them. It is over 8 h in the buffer gas at a flow rate of 2 scft min^{-1} before there is no further variation in the lattice parameters (see Figure 11b). This illustrates that oxygen diffusion throughout the sample is relatively slow and results, upon cooling of the oxygen-deficient, as-made material during synthesis, in the inhomogeneous oxygen distribution, which gives rise to the multiphasic behavior observed.

We hoped to gain insight into precisely how the oxygen vacancies relocated within the unit cell by collecting data at 5 °C intervals in the range $300 \leq T/°C \leq 460$ while heating the as-made $x = 0.6$ sample through the orthorhombic to tetragonal structural transition. Unfortunately, because of the broad nature of the transition, we found it impossible to extract any quantitative information from the data collected, other than that the transition appears to occur over a wide temperature region, rather than in a sharp step. It is difficult to determine whether this broadness is a feature intrinsic to the sample itself, resulting perhaps from the multiphasic, inhomogeneous nature of the room-temperature material already discussed, or due to extrinsic effects introduced by the experimental conditions. The Miller furnace apparatus employed for the in situ heating experiments necessitates use of a pelletized sample. This raises concerns over the oxygen diffusion rate and the possible introduction of temper-

Table 4. Mn−O Bond Lengths (Å) Obtained from Rietveld Refinement of Room-Temperature and 600 °C Powder Neutron Diffraction Data, for $x = 0.6$ and $x = 0.7$ $Nd_{2-2x}Sr_{1+2x}Mn_2O_{7+\delta}$ Samples As-Made at 1400 °C in 0.507% CO/19.63% CO_2 in N_2 ($\delta < 0$), and Also Subsequently Oxygen Annealed at 500 °C ($\delta = 0$)

sample	0.6	0.6	0.6	0.7	0.7	1.0[a]	1.0[a]
Mn oxidation state	+3.60	+3.07	+3.60	+3.13	+3.70	+3.55	+4.02
δ	0.00(1)	−0.53(1)	0.00	−0.58(1)	−0.00(1)	−0.45(1)	0.02(1)
temperature	RT	600 °C	600 °C	RT	RT	RT	RT
Mn−O(1) (×1)	1.931(3)	1.977(8)	1.956(4)	1.944(4)	1.931(3)	1.954(3)	1.951(3)
Mn−O(2) (×1)	1.934(4)	1.955(9)	1.939(6)	1.954(6)	1.925(4)	1.899(4)	1.906(4)
Mn−O(3) (×4)	1.92261(7)	1.9489(6)	1.9340(1)	1.9343(3)	1.91950(7)	1.91406(6)	1.89986(1)

[a] Data for the $x = 1.0$ composition, $Sr_3Mn_2O_{7+\delta}$, are taken from ref 26.

ature and $p(O_2)$ gradients across the material. A comparison of the data discussed above, collected on the two 9-mm-thick, 5-g pellets, with that collected for a single 0.75-g, 3-mm-thick pellet of the same material indicates that these are indeed serious issues that must be considered. The time taken at 600 °C for oxygen vacancy formation and equilibration, as adjudged by diminishing variation of the lattice constants, in the 0.507% CO/19.63% CO_2 in N_2 buffer gas for the single thin pellet, being considerably reduced compared to that for the two larger pellets, $\tau_a = 68$ and 509 min, respectively; see Figure 11a,b. Unfortunately, the increased data collection time required to achieve high-quality statistics necessary for Rietveld refinement using a smaller sample mass made it unrealistic to carry out the entire experiment using such a thin pellet.

In summary, at temperatures greater than ≈450 °C both the as-made $x = 0.6$ and $x = 0.7$ samples have vacancies in the apical O(1) position corresponding to the oxygen atom shared between the MnO octahedra in the bilayers. Upon cooling of the samples below 450 °C, the vacancies in the $x = 0.7$ material remain in the apical position. In the $x = 0.6$ material they begin to migrate to positions within the MnO_2 planes, preferentially along the *a* axis, thereby producing an orthorhombic distortion of the high-temperature structure. This vacancy migration is slow and not fully complete by room temperature, leading to an inhomogeneous multiphasic sample with vacancies in both equatorial and axial positions.

Crystal Structure. The trends in Mn−O bond lengths with both *x* and δ are consistent with the proposed oxygen vacancy structures summarized above. The Mn−O bond lengths obtained from the refinements discussed previously are given in Table 4, along with those for the $x = 1.0$ material, $Sr_3Mn_2O_{7+\delta}$, for comparison. The need to fix the atomic coordinates in each phase to be equal makes the bond lengths obtained from the multiphase, room-temperature refinement for the as-made $x = 0.6$ material meaningless for comparison and so these values are not included. As expected, the room-temperature MnO_6 octahedral volume of the $\delta = 0$ samples decreases with increasing *x*, that is, increasing Mn oxidation state. Upon oxidation of the as-made compounds, whether at room temperature ($x = 0.7$ and $x = 1.0$) or 600 °C ($x = 0.6$), all three compositions show similar contractions in the in-plane Mn−O(3) bond length of ≈0.75%, within error. For the $x = 0.6$ and $x = 0.7$ materials there are also contractions of a similar magnitude in the Mn−O(1) and Mn−O(2) axial bond lengths upon filling of the vacancies. For $x = 1.0$, however, these bonds remain effectively unchanged by the increase in Mn oxidation state.

There are two contributing factors that together give rise to the variations in bond lengths observed upon filling of the vacancies: an overall contraction in octahedral volume, expected because of the increase in Mn oxidation state, plus an anisotropic effect arising from the specific location within the octahedral bilayers of the vacancies that are filled. In the $x = 1.0$ as-made material, $Sr_3Mn_2O_{6.45}$, the oxygen vacancies are distributed randomly within the MnO_2 planes. That the axial Mn−O bonds remain essentially unchanged upon oxidation serves to illustrate the insensitivity of these bonds to not only the presence of vacancies within the plane but also the change in oxidation state. An analogous result is found upon oxidation of the oxygen-deficient, distorted $n = 1$ Ruddlesden−Popper compound $Ca_2MnO_{3.5}$, where the oxygen vacancies are ordered in the plane, resulting in a two-dimensional network of vertex-linked Mn^{3+} square pyramids.[27] No change in the axial Mn−O bond length occurs when the vacancies are filled to yield the stoichiometric $\delta = 0$ Mn^{4+} compound, Ca_2MnO_4, despite the increase in Mn oxidation state. In contrast, in $Sr_2Fe_2O_{6.58}$, where the oxygen vacancies lie in the apical O(1) position, as is predominantly found with $n = 2$ Ruddlesden−Popper phases, there is a marked decrease in the axial Fe−O(1) bond length associated with oxidation.[23] This leads us to conclude that changes in the axial Mn−O bonds upon oxidation will result only from the location of vacancies in apical positions in the MnO_6 octahedra, not from an increase in the Mn oxidation state. Despite the lack of in-plane defects in the $Sr_2Fe_2O_{6.58}$ compound, however, a contraction in the Fe−O(3) equatorial bond also occurs upon filling the apical O(1) vacancies. This observation, along with the fact that the percentage decrease in the Mn−O(3) bond length is very similar for the $x = 0.6$, $x = 0.7$, and $x = 1.0$ samples discussed here, suggests it is the increase in Mn oxidation state upon filling of the vacancies that is the dominant effect on the in-plane Mn−O bond lengths rather than the location of the vacancies themselves. Thus, apical Mn−O bonds respond only to apical vacancies while equatorial Mn−O bonds respond only to oxidation state changes. Examining the changes in Mn−O bond lengths upon oxidation based upon the above discussions suggests the existence of solely apical oxygen vacancies for the $x = 0.7$ composition and $x = 0.6$ sample at 600 °C. In view of the predominance of literature data, we suggest that these occur exclusively at the O(1) position shared between the octahedral bilayers, but because for both materials there is also significant contraction in the

(27) Leonowicz, M. E.; Poeppelmeier, K. R.; Longo, J. M. *J. Solid State Chem.* **1985**, *59*, 71.

Mn−O(2) upon filling of the vacancies, we cannot rule out the possibility of some defects at the O(2) site.

Summary

By systematically reducing the oxygen partial pressure during synthesis, we have successfully extended single $n = 2$ phase synthesis at 1400 °C in the $Nd_{2-2x}Sr_{1+2x}Mn_2O_7$ solid solution down to $x = 0.2$. We were unable, however, to directly produce stoichiometric $Nd_{2-2x}Sr_{1+2x}Mn_2O_7$ materials with $x > 0.5$, that is, with Mn in an average oxidation state greater than +3.5, at 1400 °C in any atmosphere corresponding to $3.9 \times 10^{-6} \leq p(O_2)/\text{atm} \leq 1.0$. This is consistent with our prior conclusions based upon the results for the $La_{2-2x}Sr_{1+2x}Mn_2O_{7+\delta}$ series, that $Mn^{3.5+}$ is the maximum mean oxidation state attainable directly in a layered $n = 2$ manganite system by any ambient pressure, high-temperature route.[28] As with the lanthanum strontium manganites, the use of a two-step procedure in which the formation of oxygen vacancies within the structure is followed by low-temperature oxygen annealing to yield the stoichiometric material appears essential in providing access to $Nd_{2-2x}Sr_{1+2x}Mn_2O_7$ compositions containing higher concentrations of Mn^{4+}. Such compositions may enable a more complete investigation of the interplay among structure, magnetism, and transport in layered manganites.

In contrast to the oxygen-deficient $x = 1.0$ end member of the series, $Sr_3Mn_2O_{6.55}$, produced by quenching into dry ice from 1650 °C, where the oxygen vacancies are found to be disordered within the MnO_2 planes,[26] here, for the $x = 0.6$ $\delta = -0.53$ material, ordering of the vacancies along the *a* axis during cooling from 1400 °C results in $b > a$. This is responsible for an orthorhombic *Immm* distortion of the structure observable in the room-temperature diffraction pattern. (The term "ordered" is used to indicate preferential location of the oxygen vacancies along the *a* axis of the *Immm* structure; there is no evidence for further ordering of the vacancies along that direction.) Closer inspection of the data for this sample, however, shows it to be multiphasic in nature. Although constraints of the refinement software employed realistically limit the number of phases that can be incorporated in the Rietveld refinement model to three, it is likely that the sample actually consists of a continuum of phases with subtly different oxygen concentrations and associated vacancy distributions. A greater number of vacancies order along the *a* axis within the plane, leading to a larger orthorhombic splitting of the *a* and *b* lattice parameters for a given constituent phase.

In the $x = 0.7$ material, prepared under absolutely identical conditions and containing a very similar number of vacancies to the $x = 0.6$ sample ($\delta = -0.57$ versus -0.53), the oxygen defects occur predominately in the apical position between the MnO_2 sheets rather than in the plane, and no orthorhombic distortion is observed. This further serves to illustrate the rich anion defect chemistry of these layered manganite systems. During synthesis of both the $x = 0.6$ and $x = 0.7$ materials at 1400 °C, the vacancies will be disordered; it is only upon cooling that the two contrasting defect structures are formed. Presumably, some subtle crystal structure differences between the two compositions, set at synthesis temperature, favor the ordering of vacancies in the $x = 0.6$ material, but not in the $x = 0.7$ material. Unfortunately, we have been unable to verify this hypothesis. Establishing the underlying cause of the apparently large variations in defect behavior in conjunction with what appear to be relatively minor changes in composition remains a challenge in understanding the crystal chemistry of these phases.

Acknowledgment. The authors thank Simine Short for assistance with the TOF powder neutron diffraction measurements. This work was supported by the U.S. Department of Energy, Basic Energy Sciences-Materials Sciences under Contract W-31-109-ENG-38 (J.E.M., J.F.M.).

CM990809E

(28) Millburn, J. E.; Mitchell, J. F.; Argyriou, D. N. *Chem. Commun.* **1999**, *15*, 1389−1390.